

Bimetallic Aerogels: High-Performance Electrocatalysts for the Oxygen Reduction Reaction**

Wei Liu, Paramaconi Rodriguez, Lars Borchardt, Annette Foelske, Jipei Yuan, Anne-Kristin Herrmann, Dorin Geiger, Zhikun Zheng, Stefan Kaskel, Nikolai Gaponik, Rüdiger Kötz, Thomas J. Schmidt,* and Alexander Eychmüller*

Metallic nanomaterials with high surface area and high porosity are of great interest for applications in catalysis, electrochemistry, and sensors. Several strategies have been developed for preparing porous metallic nanostructures, for instance, templating,^[1,2] combustion synthesis,^[3] cathodic corrosion,^[4] and by forming aerogels.^[5–10] Aerogels are a unique class of materials that present low densities, large open pores, and high inner surface areas. Some aerogel materials have physical and chemical properties that are superior to those of conventional nanoparticles since the specific properties of the nanomaterials are combined and magnified by self-assembly on the macroscale.^[8,11] Among the different methods of preparing metallic aerogels,^[5–10] we have developed a spontaneous method for the synthesis of Pd aerogels through the reduction of K_2PdCl_4 in the presence of different cyclodextrins.^[8] The cyclodextrin-modified Pd aerogels have shown excellent performance in the electrocatalysis of ethanol oxidation. Thus, the exploration of novel metallic aerogels and their applications are of great interest.

One potential application of metallic aerogels is as unsupported catalysts in low-temperature polymer electrolyte fuel cells (PEFCs), in particular as cathode materials for the oxygen reduction reaction (ORR). Currently the lifetime of the fuel cells is limited by the carbon supports employed due to corrosion, for example, during start–stop cycling or idling conditions. In recent years unsupported catalysts for PEFCs have been mainly promoted by the company 3M and both the high activity and the durability of their unique nanostructured thin-film (NSTF) catalysts/electrodes have been demonstrated.^[12] Although these nanostructures showed high spe-

cific catalytic activity and durability with a low loading of the noble metal, the maximum specific surface area of $20\text{--}30\text{ m}^2\text{ g}^{-1}$ imposes some limitations.^[13] Therefore, extended unsupported electrocatalysts offering higher specific surface areas are desirable in order to further increase the overall catalyst activity and maintain high stabilities. The use of metallic aerogel catalysts presents a suitable way to achieve these goals.


Pt-based nanomaterials are still the most effective catalysts for the ORR, but the platinum mass activity must be further increased by at least a factor of 4 if cost targets for the application of PEFC systems in automobiles are to be met.^[14] There have been various approaches to overcome the sluggish ORR kinetics, for example by shaping the Pt-based catalysts into nanowires, nanotubes, nanocrystals, and porous nanosponges,^[15–18] by controlling the size of the Pt nanoparticles at the optimum of around 2–5 nm,^[19,20] and by adjusting the composition of the Pt-based nanomaterials in the form of bimetallic or multimetallic catalysts. Pt–M (M = Pd, Co, Ni, Fe, Au, Cu, etc.) bimetallic catalysts have been confirmed to show improved ORR activity due to the change of the surface composition and electronic structure which helps to optimize the binding energy between Pt and the oxygenated species.^[14,21–25] The most intriguing Pt–M bimetallic catalyst for the ORR reported so far is $Pt_3Ni(111)$, which shows a 90-fold higher specific activity than Pt/C.^[24] The typical factor of improvement for carbon-supported PtNi systems versus Pt/C catalysts, however, is only 2–5.^[14,24,26] Another challenge can be found in the limited durability of the cathode catalysts during load cycling, which is caused by the dissolution and/or

[*] Dr. W. Liu, Dr. J. Yuan, A.-K. Herrmann, Dr. N. Gaponik, Prof. A. Eychmüller
Physical Chemistry, TU Dresden
Bergstrasse 66b, 01062 Dresden (Germany)
E-mail: alexander.eychmueller@chemie.tu-dresden.de
Homepage: <http://www.chm.tu-dresden.de/pc2/>
Dr. P. Rodriguez, Dr. A. Foelske, Dr. R. Kötz, Prof. T. J. Schmidt
Paul Scherrer Institut, Electrochemistry Laboratory
5232 Villigen PSI (Switzerland)
E-mail: thomasjustus.schmidt@psi.ch
Homepage: <http://www.psi.ch/lec/>
Dr. P. Rodriguez
School of Chemistry, The University of Birmingham
Birmingham B15 2TT (UK)
Dr. L. Borchardt, Prof. S. Kaskel
Inorganic Chemistry, TU Dresden
Bergstrasse 66b, 01062 Dresden (Germany)

Dr. D. Geiger^[†]
Triebenberg Laboratory for HRTEM and Electron Holography
Institute for Structure Physics, TU Dresden
Zum Triebenberg 50, 01328 Dresden (Germany)
Dr. Z. Zheng
ETH Zürich, Institut für Polymere, HCI G 525
Wolfgang-Pauli-Strasse 10, 8093 Zürich (Switzerland)

[†] Current address: University of Ulm
Electron Microscopy Group of Materials Science (Germany)

[**] W.L. and J.Y. acknowledge support from the Alexander von Humboldt Foundation. This research was funded by the DFG (EY 16/10-2).

 Supporting information for this article is available on the WWW under <http://dx.doi.org/10.1002/anie.201303109>.

agglomeration of Pt and the corrosion of the carbon support. In this context, extended Pt-black-type catalysts were found to offer significantly higher voltage cycling stability than Pt nanoparticles.^[13] Although common Pt/C catalysts are industrially available, simple and environmentally friendly methods for the synthesis of advanced nanocrystal catalysts, which should be suitable for scaling up, are urgently required.

In this context, we prepared nanostructured Pt and Pd monometallic and Pt_xPd_y bimetallic aerogels with controlled composition and very high surface area and high porosity (see the Experimental Section and Figure S1 in the Supporting Information). The scanning electron microscopy (SEM) and transmission electron microscopy (TEM) images (Figure 1 a–c) show that the Pt₅₀Pd₅₀ aerogel has a three-dimensional

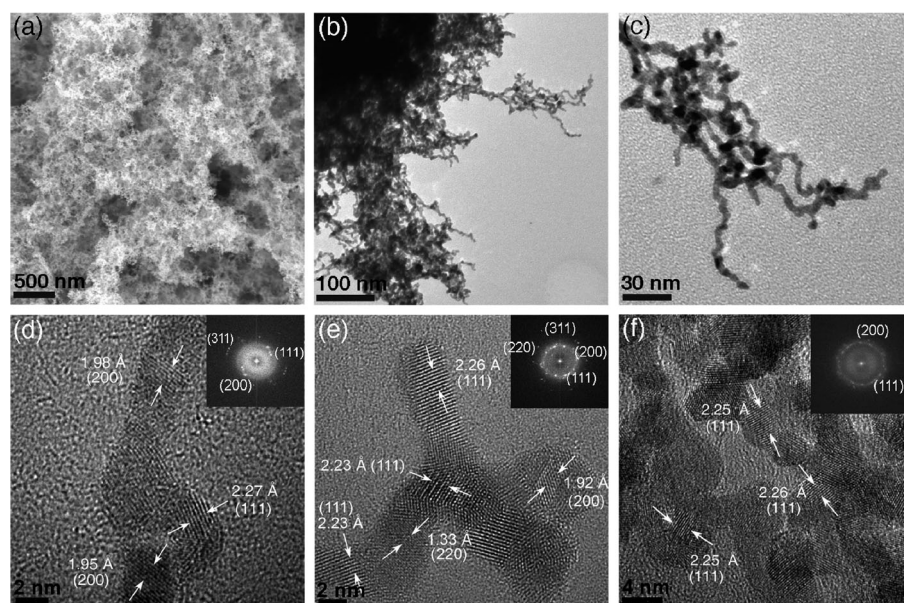


Figure 1. SEM image (a) and TEM images (b,c) of the Pt₅₀Pd₅₀ aerogel at different magnifications. HRTEM images of one nanowire in the Pt₅₀Pd₅₀ aerogel with a free branch (d), one cross-linked end (e), and one cross-linked area (f). The insets are their corresponding fast Fourier transformations (FFT).

porous network structure composed of ultrathin primary nanowires with an average diameter of 4.2 nm. These primary nanowires are fused and interconnected forming a branch-type structure. High-resolution TEM (HRTEM) images and the corresponding FFTs of the Pt₅₀Pd₅₀ aerogel (Figure 1 d–f) reveal that the Pt₅₀Pd₅₀ nanowire networks are highly crystalline with a face-centered cubic (fcc) polycrystalline structure. The crystalline domains containing lattice planes with interplanar distances of about 2.26 Å are assigned to the (111) plane of fcc metallic Pt₅₀Pd₅₀, and are widely distributed on the aerogel.

The corresponding analysis on the other bimetallic aerogels and the monometallic aerogels was performed as presented in Figures S2 and S3 in the Supporting Information. The average diameter of the nanowires in the Pt_xPd_y aerogels is not strongly influenced by the Pt/Pd ratios in the samples (Figure S4).

The compositions of the Pt_xPd_y aerogels were determined by using energy-dispersive X-ray spectroscopy (EDS) and X-ray photoelectron spectroscopy (XPS) (Figure S5 and Table S1 in the Supporting Information). The results indicate that the contents of Pt and Pd in the Pt_xPd_y aerogels are in agreement with the ratio of metal precursors during the synthesis. XPS was further used to determine the surface composition and the d-band center of the Pt_xPd_y aerogels. The survey spectrum of the Pt₅₀Pd₅₀ aerogel (Figure S6) indicates that there is mainly Pt, Pd, O, and trace amounts of C contamination in the aerogel. Deconvolution of the high-resolution Pt 4f and Pd 3d core-level spectra for the Pt_xPd_y aerogels show that both of them include two sets of peaks (Figure S7). One set shows Pd 3d_{5/2} at 335.2 eV and Pd 3d_{3/2} at 340.5 eV, and Pt 4f_{7/2} at 71.0 eV and Pt 4f_{5/2} at 74.3 eV; these values are in accordance with those for Pd⁰ and Pt⁰, respectively.^[27] The other set includes Pd 3d_{5/2} at 337.1 eV and Pd 3d_{3/2} at 342.4 eV, and Pt 4f_{7/2} at 72.6 eV and Pt 4f_{5/2} at 75.9 eV, which are close to the reported values for Pd^{II} and Pt^{II}, respectively.^[20,27–30] The deconvolution results suggest that about 80% of the Pt and Pd elements in the Pt_xPd_y aerogels are Pt⁰ and Pd⁰. The shoulder peak at around 331.9 eV next to the Pd 3d_{5/2} signal is related to the core-level spectrum for Pt 4d_{3/2}.^[27,31]

The surface area and porosity of the Pt_xPd_y, Pd, and Pt aerogels were determined from N₂ physisorption isotherms (Figure 2). The surface area as estimated from a Brunauer–Emmett–Teller (BET) plot is 73 m² g^{−1}, 86 m² g^{−1}, 75 m² g^{−1}, 125 m² g^{−1}, and 168 m² g^{−1} for the Pt₈₀Pd₂₀, Pt₅₀Pd₅₀, Pt₂₀Pd₈₀, Pd, and Pt aerogels, respectively. The pore size distribution of these aerogels

was assessed using the Barrett–Joyner–Halenda (BJH) method. All the tested aerogels show the presence of a broad range of pores from micropores (<2 nm) to mesopores (2–50 nm). The absence of a plateau at high relative pressure (*P*/*P*₀) in the adsorption isotherm implies the simultaneous presence of macropores (pore diameter > 50 nm). The presence of meso- and macropores in the aerogel is also evident in the SEM and TEM images. Notably, there is a difference in the pore size distributions for the Pt_xPd_y aerogels and the Pt and Pd aerogels. The Pt_xPd_y aerogels contain more mesopores larger than 20 nm (Table S2) and fewer micropores than the Pt and Pd aerogels. In addition, the cumulative pore volumes for pores smaller than 140 nm in the Pt_xPd_y aerogels are larger than those in Pt and Pd aerogels (Table S2). The higher porosity and the existence of more mesopores exceeding 25 nm in the Pt_xPd_y aerogels minimizes

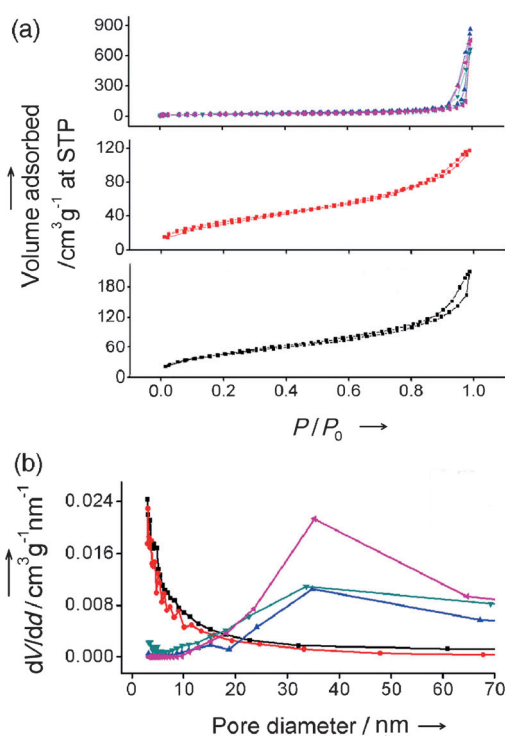


Figure 2. N₂ physisorption isotherms (a) and pore size distribution (b) determined from the isotherms using the BJH method for the Pt₈₀Pd₂₀ (green), Pt₅₀Pd₅₀ (blue), Pt₂₀Pd₈₀ (pink), Pd (red), and Pt (black) aerogels.

Knudsen diffusion and therefore minimizes the diffusion resistances in the catalyst layer of PEFC cathodes.^[14]

After the physical characterization, the monometallic and bimetallic Pt_xPd_y aerogels were evaluated as ORR catalysts (see the Tafel plots for the different Pt_xPd_y alloys alongside with the Pt/C reference system in Figure S8). The specific activity (based on total metal loading) at 0.9 V as a function of Pt content in the alloys is shown in Figure 3a. Volcano-type behavior can be seen, with the Pt₈₀Pd₂₀ aerogel at the top. The downshift of the d-band center in the alloys is commonly used to describe the oxygen reduction activity which shows the same trend (Figure 3b); for Pt₈₀Pd₂₀ DFT calculations predict that the d-band center shifts from roughly 0.1 eV to 0.2 eV.^[32] The remarkable activity of the Pt₈₀Pd₂₀ aerogel in the volcano plot indicates the best balance between the free energies of adsorption of O₂ and the surface coverage by spectator (blocking) species and intermediates.^[33]

Comparison of the activities of the Pt_xPd_y aerogels with that of the Pt/C reference (20 wt %) clearly indicates that Pt_xPd_y bimetallic aerogels are highly active catalysts for PEFC cathodes. The Pt_xPd_y bimetallic aerogels containing more than 40 % Pt meet or exceed the performance targets for ORR fuel cell catalysts (0.44 A mg⁻¹ Pt at 0.9 V versus RHE and 80 °C) set by the U.S. Department of Energy.^[14]

Durability tests were performed by applying linear potential sweeps between 0.5 and 1.0 V at 50 mV s⁻¹ in O₂-saturated 0.1 M HClO₄ solutions at room temperature, simulating the typical voltage range of a fuel cell cathode under automotive drive cycle conditions. The test results for the Pt,

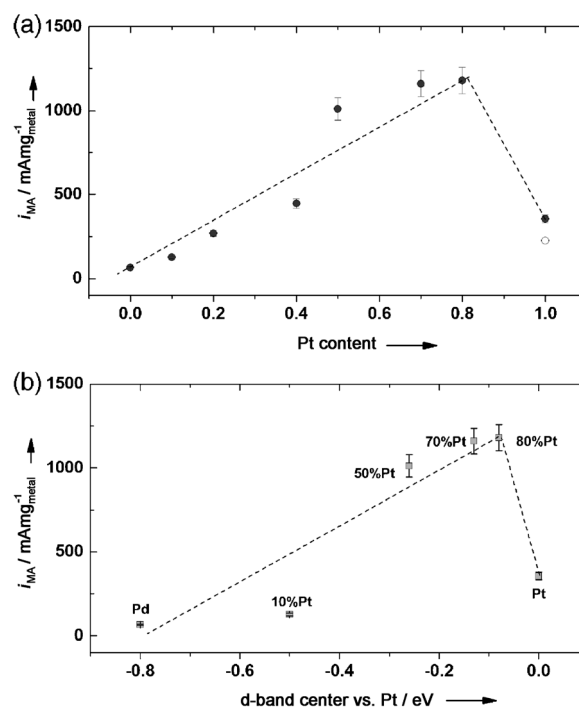


Figure 3. a) Volcano plots of the ORR mass activity of the Pt_xPd_y, Pt, and Pd aerogel catalysts as a function of Pt content at 0.9 V. The empty circle represents the value for Pt/C. b) Volcano plots of the ORR mass activity at 0.9 V of the aerogel catalysts as a function of the shift of the d-band center from that of the Pt aerogel calculated from valence-band XPS measurements.

Pt₈₀Pd₂₀, Pt₄₀Pd₆₀, and Pd aerogels and for Pt/C are shown in Figure 4. The mass activities of the Pt, Pd, and Pt/C materials decrease gradually with time. In contrast, for the Pt₈₀Pd₂₀ and Pt₄₀Pd₆₀ aerogels the mass activity first increases and then decreases slowly. The commercial Pt/C catalyst (isolated Pt nanoparticles; 54 % loss after 10000 cycles) and the Pt aerogel (Pt nanoparticle networks; 56 % loss) show similar durability

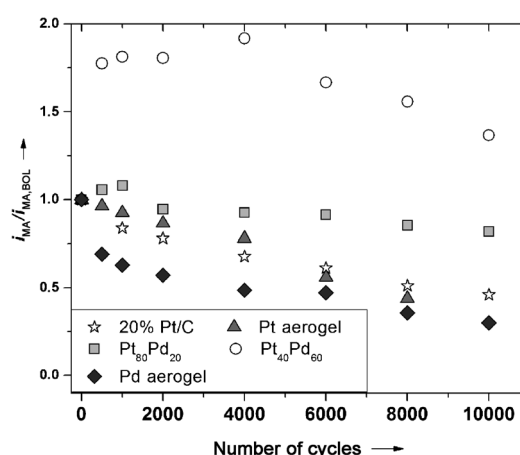


Figure 4. Relative ORR mass activity of Pt_xPd_y catalysts of different compositions as a function of the number of potential cycles (0.5 V to 1.0 V). The mass activity was obtained from the cathodic scan of ORR polarization curves (corrected for electrolyte resistances) at 10 mV s⁻¹ and 1600 rpm.

in this test. The Pt₈₀Pd₂₀ (12 % loss) and Pt₄₀Pd₆₀ (36 % increase) bimetallic aerogels show much better durability than the pure Pt and Pd aerogels well as Pt/C, indicating that the existence of Pd in Pt_xPd_y alloy aerogels significantly stabilizes the catalyst. The significant enhancement of mass activity upon potential cycling for the high-Pd-content Pt_xPd_y alloy aerogels, for example, Pt₄₀Pd₆₀, is supposed to be due to the de-alloying of Pd upon potential cycling such that it slowly approaches the behavior of the Pt-rich aerogel alloys. This type of behavior was also reported for PtCu₃ and PtNi₃ alloys.^[34]

In summary, we have presented an environmentally benign strategy for the controllable synthesis of bimetallic Pt_xPd_y and monometallic Pt and Pd aerogels, and for the first time, noble-metal-alloy aerogels (Pt_xPd_y) have been demonstrated to be highly active and stable catalysts for PEFC cathodes. The Pt_xPd_y aerogels are composed of three-dimensional nanowire network structures and display very high surface area and large porosity. They show excellent electrocatalytic activity towards the oxygen reduction reaction, with the Pt₈₀Pd₂₀ aerogel performing the best and showing five times higher mass activity than the commercial Pt/C catalyst.

Notably, the Pt_xPd_y aerogels also show excellent durability during the test. The metallic aerogels have potential as electrocatalyst systems that combine the high stability of extended surfaces and the high surface area of nanoparticles. They are very promising as a new class of catalysts not only for PEFCs but also for other electrochemical energy systems.

Received: May 3, 2013

Published online: July 22, 2013

Keywords: aerogels · electrocatalysis · oxygen reduction reaction · palladium · platinum

- [1] G. W. Nyce, J. R. Hayes, A. V. Hamza, J. H. Satcher, Jr., *Chem. Mater.* **2007**, *19*, 344–346.
- [2] J. Erlebacher, M. J. Aziz, A. Karma, N. Dimitrov, K. Sieradzki, *Nature* **2001**, *410*, 450–453.
- [3] B. C. Tappan, M. H. Huynh, M. A. Hiskey, D. E. Chavez, E. P. Luther, J. T. Mang, S. F. Son, *J. Am. Chem. Soc.* **2006**, *128*, 6589–6594.
- [4] A. I. Yanson, P. Rodriguez, N. Garcia-Araez, R. V. Mom, F. D. Tichelaar, M. T. M. Koper, *Angew. Chem.* **2011**, *123*, 6470–6474; *Angew. Chem. Int. Ed.* **2011**, *50*, 6346–6350.
- [5] N. Leventis, N. Chandrasekaran, A. G. Sadekar, C. Sotiriou-Leventis, H. Lu, *J. Am. Chem. Soc.* **2009**, *131*, 4576–4577.
- [6] N. Leventis, N. Chandrasekaran, A. G. Sadekar, S. Mulik, C. Sotiriou-Leventis, *J. Mater. Chem.* **2010**, *20*, 7456–7471.
- [7] N. C. Bigall, A.-K. Herrmann, M. Vogel, M. Rose, P. Simon, W. Carrillo-Cabrera, D. Dorfs, S. Kaskel, N. Gaponik, A. Eychmüller, *Angew. Chem.* **2009**, *121*, 9911–9915; *Angew. Chem. Int. Ed.* **2009**, *48*, 9731–9734.
- [8] W. Liu, A.-K. Herrmann, D. Geiger, L. Borchardt, F. Simon, S. Kaskel, N. Gaponik, A. Eychmüller, *Angew. Chem.* **2012**, *124*, 5841–5846; *Angew. Chem. Int. Ed.* **2012**, *51*, 5743–5747.
- [9] B. C. Tappan, S. A. Steiner III, E. P. Luther, *Angew. Chem.* **2010**, *122*, 4648–4669; *Angew. Chem. Int. Ed.* **2010**, *49*, 4544–4565.
- [10] S. Ye, A. K. Vijh, Z.-Y. Wang, L. H. Dao, *Can. J. Chem.* **1997**, *75*, 1666–1673.
- [11] H. D. Gesser, P. C. Goswami, *Chem. Rev.* **1989**, *89*, 765–788.
- [12] M. K. Debe, *Nature* **2012**, *486*, 43–51.
- [13] M. K. Debe, *ECS Trans.* **2012**, *45*, 47–68.
- [14] A. Rabis, P. Rodriguez, T. J. Schmidt, *ACS Catal.* **2012**, *2*, 864–890.
- [15] C. Koenigsmann, W.-P. Zhou, R. R. Adzic, E. Sutter, S. S. Wong, *Nano Lett.* **2010**, *10*, 2806–2811.
- [16] C. Wang, H. Daimon, T. Onodera, T. Koda, S. Sun, *Angew. Chem.* **2008**, *120*, 3644–3647; *Angew. Chem. Int. Ed.* **2008**, *47*, 3588–3591.
- [17] J. X. Wang, C. Ma, Y. Choi, D. Su, Y. Zhu, P. Liu, R. Si, M. B. Vukmirovic, Y. Zhang, R. R. Adzic, *J. Am. Chem. Soc.* **2011**, *133*, 13551–13557.
- [18] H. Atae-Esfahani, Y. Nemoto, L. Wang, Y. Yamauchi, *Chem. Commun.* **2011**, *47*, 3885–3887.
- [19] F. J. Perez-Alonso, D. N. McCarthy, A. Nierhoff, P. Hernandez-Fernandez, C. Streb, I. E. L. Stephens, J. H. Nielsen, I. Chorkendorff, *Angew. Chem.* **2012**, *124*, 4719–4721; *Angew. Chem. Int. Ed.* **2012**, *51*, 4641–4643.
- [20] K. Yamamoto, T. Imaoka, W. J. Chun, O. Enoki, H. Katoh, M. Takenaga, A. Sonoi, *Nat. Chem.* **2009**, *1*, 397–402.
- [21] C. Wang, N. M. Markovic, V. R. Stamenkovic, *ACS Catal.* **2012**, *2*, 891–898.
- [22] B. Lim, M. Jiang, P. H. C. Camargo, E. C. Cho, J. Tao, X. Lu, Y. Zhu, Y. Xia, *Science* **2009**, *324*, 1302–1305.
- [23] C. Koenigsmann, A. C. Santulli, K. Gong, M. B. Vukmirovic, W. Zhou, E. Sutter, S. S. Wong, R. R. Adzic, *J. Am. Chem. Soc.* **2011**, *133*, 9783–9795.
- [24] V. R. Stamenkovic, B. Fowler, B. S. Mun, G. F. Wang, P. N. Ross, C. A. Lucas, N. M. Markovic, *Science* **2007**, *315*, 493–497.
- [25] J. W. Hong, S. W. Kang, B. S. Choi, D. Kim, S. B. Lee, S. W. Han, *ACS Nano* **2012**, *6*, 2410–2419.
- [26] T. J. Schmidt, *ECS Trans.* **2012**, *45*, 3–14.
- [27] B. Veisz, L. Tóth, D. Teschner, Z. Paál, N. Györfy, U. Wild, R. Schlögl, *J. Mol. Catal. A* **2005**, *238*, 56–62.
- [28] J.-S. Lim, S.-M. Kim, S.-Y. Lee, E. A. Stach, J. N. Culver, M. T. Harris, *Nano Lett.* **2010**, *10*, 3863–3867.
- [29] Y. Xiong, H. Cai, B. J. Wiley, J. Wang, M. J. Kim, Y. Xia, *J. Am. Chem. Soc.* **2007**, *129*, 3665–3675.
- [30] S. Wang, S. P. Jiang, T. J. White, J. Guo, X. Wang, *J. Phys. Chem. C* **2009**, *113*, 18935–18945.
- [31] B. I. Boyanov, T. I. Morrison, *J. Phys. Chem.* **1996**, *100*, 16318–16326.
- [32] V. Stamenkovic, B. S. Mun, K. J. J. Mayrhofer, P. N. Ross, N. M. Markovic, J. Rossmeisl, J. Greeley, J. K. Nørskov, *Angew. Chem.* **2006**, *118*, 2963–2967; *Angew. Chem. Int. Ed.* **2006**, *45*, 2897–2901.
- [33] V. R. Stamenkovic, B. S. Mun, M. Arenz, K. J. J. Mayrhofer, C. A. Lucas, G. Wang, P. N. Ross, N. M. Markovic, *Nat. Mater.* **2007**, *6*, 241–247.
- [34] “Dealloyed Pt alloy electrocatalysts for the Oxygen Reduction Reaction”: P. Strasser in *Handbook of Fuel Cells: Advances in Electrocatalysis, Materials, Diagnostics, and Durability* (Eds.: W. Vielstich, H. Yokokawa, H. A. Gasteiger), Wiley, New York, **2009**, p. 30.